Article

A Model to Study Thermal Energy Delivery to the Choroid: A Comparison of Surgical Devices

Stephen A. LoBue[1,2], Prashant Tailor[3], Jarel K. Gandhi[1], Paul Loftness[4], and Timothy W. Olsen[1,2]

[1] Department of Ophthalmology, Mayo Clinic, Rochester, MN, USA
[2] Department of Ophthalmology, Emory University, Atlanta, GA, USA
[3] Medical College of Georgia, Augusta, GA, USA
[4] University of Minnesota, Minneapolis, MN, USA

Purpose: We measure and compare surgical devices using an ex vivo, temperature-controlled, choroidal incision model during thermal energy transfer with a high-resolution infrared camera.

Methods: Ex vivo porcine choroidal tissue specimens ($n = 516$) were isolated and placed on a temperature-regulated (37°C) perfusion platform. We tested the pulsed electron avalanche knife (PEAK), micropulse laser (MpL), continuous laser (CL), and bipolar cautery (BpC) at three energy settings (11 [low], 45 [medium], and 134 [high] mJ/mm). Each device was clamped to a stationary mechanical arm. Movement of tissue specimens beneath the surgical device was achieved using a stepping motor-driven x-y table. An infrared video camera measured orthogonal temperature variation in the surrounding tissue.

Results: Increased power resulted in greater lateral thermal spread using all modalities ($P < 0.001$). Mean (standard deviation) lateral thermal spread at low energy was smallest for the MpL at 0.0 (0.01) mm ($P < 0.001$), whereas BpC had the least collateral tissue damage at medium and high energies (0.02 [0.08] and 0.34 [0.22] mm, respectively; $P < 0.001$). Fluidics of the ex vivo system may limit thermal spread. The PEAK had the greatest thermal spread across all energy groups ($P < 0.001$), with clinically relevant variation between disposable blades.

Conclusions: Our ex vivo model enabled direct comparison of threshold thermal tissue injury across four devices. MpL and BpC showed the least thermal damage. PEAK had a higher variation in energy delivery, but also has the advantage of more effective tissue cutting.

Translational Relevance: Our ex vivo surgical device analysis provides thermal tissue injury predictions for choroidal surgery.

Introduction

The choroid is a highly vascular tissue that provides approximately 85% of the intraocular blood flow.[1] Choroidal blood flow serves a vital role in choroidal and retinal thermoregulation and is controlled by a sophisticated, light-stimulated, increased temperature feedback loop.[2,3] Choroidal anatomy is highly anastomotic and divided into three blood vessel layers: choriocapillaris, Sattler, and Haller layers. Rapid choroidal perfusion[4] helps provide nutrients and oxygen via diffusion through the Bruch membrane to meet the high metabolic demands of the retinal pigment epithelium (RPE) and retinal photoreceptors.

Given that choroidal tissue is highly vascular, any attempt to perform a controlled, surgical incision through this delicate tissue poses a substantial risk of intraocular bleeding. For example, subretinal hemorrhage may occur with drainage of subretinal fluid during scleral buckling surgery. Drainage typically is facilitated by passing a needle to puncture the

choroid, Bruch membrane, and RPE complex (CBR) and is the point of greatest hemorrhagic risk.[5] Other surgical procedures that require incision of CBR tissue include diagnostic choroidal or chorioretinal biopsy, endoresection of tumors, translocation procedures, or during repair of traumatic globe injuries. Incisional choroidal translocation surgery allows vitreoretinal surgeons to optimize and perhaps redirect choroidal blood flow to the outer macular retinal tissue, as well as regenerate metabolic support provided by the RPE. Systematically studying and optimizing the techniques and technology for incisional choroidal surgery is an exciting new area for exploration.

Surgical devices that deliver thermal energy have been proposed as a means to optimize hemostasis when creating full-thickness CBR incisions. Applying thermal energy to the choroid to establish hemostasis also may lead to collateral thermal injury of delicate adjacent tissues and structures. Thus, balancing the risks and benefits of thermal delivery during choroidal surgery is important. Standard surgical devices used to deliver noninci-sional thermal energy in ophthalmology include bipolar cautery (BpC), micropulse laser (MpL), and continuous laser (CL). The pulsed electron avalanche knife (PEAK; PlasmaBlade; Medtronic, Dublin, Ireland) is a newer technology, initially developed for tractionless tissue cutting in vitreo-retinal surgery, but this technology is not yet commercially available for ophthalmologic use. The PEAK is approved for applications in general surgery and has gained broad acceptance. In contrast to the other three technologies, PEAK is the only one capable of hemostasis and tissue cutting.

To evaluate these commonly used surgical devices and their potential for thermal damage, we developed a thermally controlled, ex vivo, air-fluid environment that simulates the temperature-buffering effects of the rapid choroidal blood flow. We measured the thermal spread from these devices using sophisticated thermal detection, sensitive to detect critical threshold temperatures for cell survival ($\leq 49°C$, above which cell death has been demonstrated),[6,7] with the goal of developing a better method for incisional choroidal surgery in vivo that optimizes hemostasis and reduces collateral thermal tissue damage. We hypothesized that each technology (PEAK, MpL, CL, and BpC) would have differing thermal effects on the choroidal tissue when delivering thermal energy.

Methods

Surgical Model

A circular, stainless steel plate served as a platform for thermal testing. The plate temperature was controlled by pumping distilled water through a polyvinyl chloride chamber sandwiched between circular stainless steel plates (Figs. 1A, 1B). A peristaltic pump (7545-00; Cole-Parmer, Vernon Hills, IL) was used to circulate fluid from a 1-gallon container warmed on a hot plate. Heating of the platform maintained the surface temperature of the tissue at 37°C. The surface temperature was calibrated using an A655SC forward-looking infrared camera (FLIR; FLIR Systems, Inc., Wilsonville, OR) placed 50 cm above the tissue (Fig. 1C).

Thermal testing was performed using the PEAK, MpL (10% duty cycle; Iridex, Mountain View, CA), CL (Iridex), and BpC (Accurus 400VS; Alcon, Ft. Worth, TX). Each device was attached to a mechanical arm (Fig. 1C) mounted above the thermal platform at a 45° angle. A micromechanical height adjuster was used to control the height of the device above the tissue (Fig. 1D) for standardization and to optimize the repeatability of thermal delivery for each device, while also minimizing tissue dragging. The tissue was kept moist in a room air environment.

Thermal Energy Delivery

The power output for each device (Table 1) was calculated in watts (W), converted to mJ/s, and standardized for net energy output equivalence between devices by adjusting the rate of device movement across the tissue. Energy delivery was corrected for consistent power delivery by determining the specific duty cycle for each modality and equivalently comparing total energy output for consistency between devices. As above, calculations of energy output were equalized by adjusting the tissue velocity (Table 1). A programmable stepping motor controller (NEAT-310) generated the precise velocity for moving the tissue platform relative to the fixed instruments. As a result, three energy levels were tested: 11.2 (low), 44.8 (medium), and 134.4 mJ/mm (high), with standardized energy output from the PEAK, MpL, CL, and BpC.

All studies were conducted with Emory University Institutional Animal Care and Use Committee approval (exemption) and in compliance with the ARVO Animal Statement for the Use of Animals in
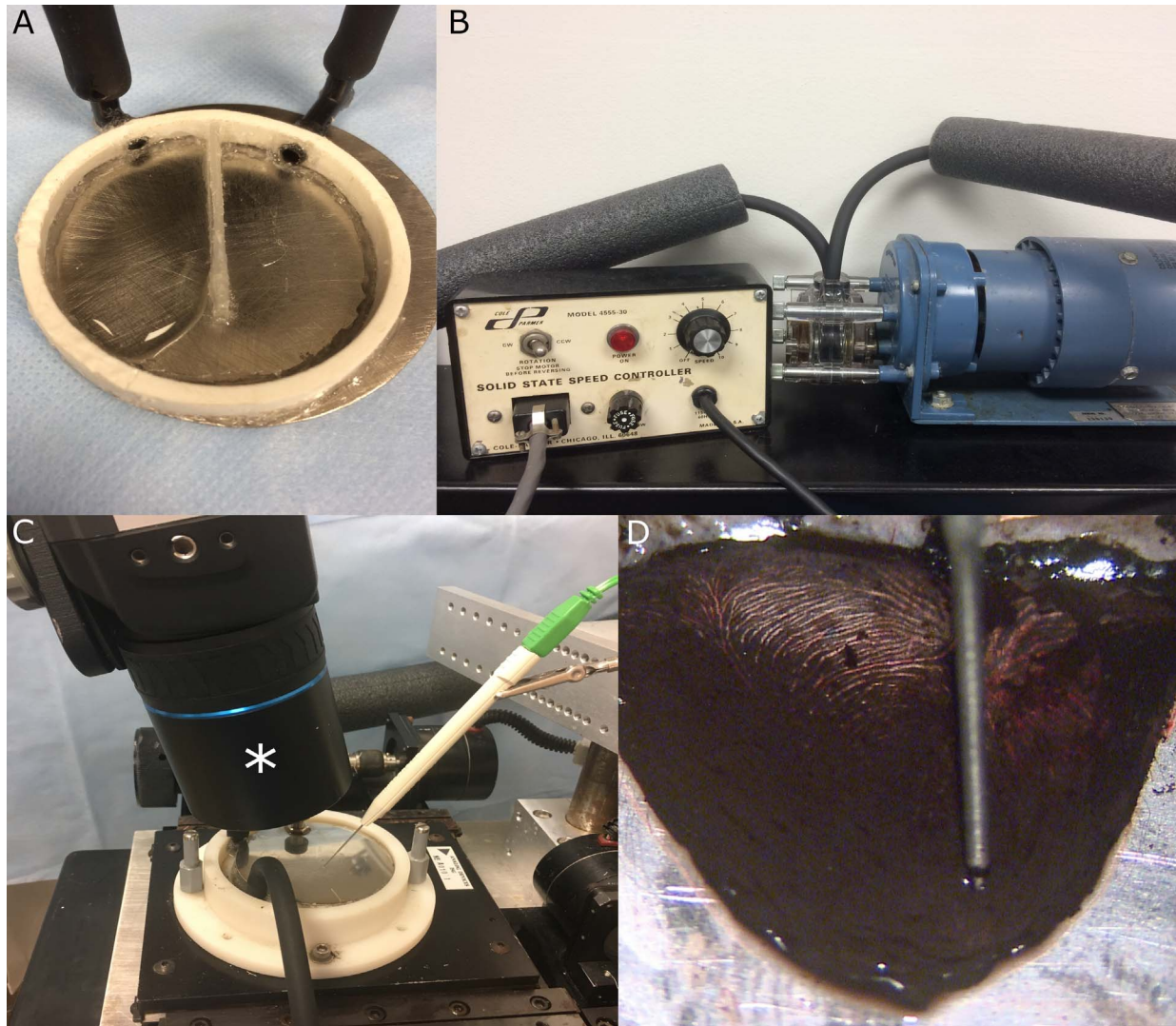
Figure 1. Experimental Setup. (A) Two pieces of circular stainless steel are sealed with polyvinyl chloride to create a chamber for fluid circulation and temperature regulation. (The *top plate* is removed to show the chamber below.) A flow control partition aids in optimizing fluid and heat distribution. (B) A peristaltic pump with a 600-RPM motor and pump head (Cole Parmer 7545-00 and 7015) is attached to enable fluid flow through the chamber. The flow rate was controlled by a Masterflex solid-state controller. Fluid was drawn from a 1-gallon water reservoir heated on a hot plate (Fisher Scientific, Hampton, NH). Tubing was insulated with polyethylene foam. (C) Cutting instruments were fixed to a mechanical arm with a 45° angle relative to the tissue plane. A microadjuster was used to standardize the height of the device tip above the tissue. A stepping motor–driven x-y table moved each specimen at a precise, controlled rate. An A655SC infrared camera (*FLIR) was mounted 50 cm above the tissue. (D) Each CBR tissue section was dissected and quartered from donor globes. After dissection and immediately before testing, the tissue was suspended in temperature-controlled balanced salt solution to prevent folding and desiccation. Once mounted on the platform, a small amount of balanced salt solution was used to keep the CBR tissue moist, but the environment was in room air.

Ophthalmic and Vision Research. Porcine eyes ($n =$ 155) were shipped to the laboratory on ice, in saline-moistened containers, within 24 hours after death and maintained at 2°C to 4°C before dissection. Globes were transected in a coronal plane using a razor blade and curved scissors to remove the anterior segment. The vitreous was removed. A microforceps and curved scissors were used to gently remove the neurosensory retina and expose the underlying RPE. The tissue was rinsed gently with balanced salt solution to remove additional tissue debris. Each CBR complex was dissected from the sclera and was cut into four, flat-mount quadrants. Samples were excluded if tissue dragging occurred (due to suboptimal probe height) or if the BpC failed to make contact with at least 30% of the sample, as observed by the

Table 1. Energy Distribution and Thermal Spread

Energy Group	Device	No. of Samples	Power at Device Tip, mJ/s	Duty Cycle, %	Velocity, mm/s	Power per mm, mJ/mm	Mean (SD) Thermal Spread at Threshold
Low	PEAK	35	500	2.24	1.00	11.2	0.23 (0.15)
	MpL	49	12	10	1.07	11.2	0.00 (0.01)
	CL	52	120	100	1.07	11.2	0.05 (0.05)
	BpC	NA	221.3	100	19.8[a]	11.2	NA[a]
Medium	PEAK	60	2000	2.24	1.00	44.8	0.97 (0.31)
	MpL	44	500	10	1.12	44.8	0.32 (0.08)
	CL	49	50	100	1.12	44.8	0.34 (0.10)
	BpC	51	221.3	100	4.94	44.8	0.02 (0.08)
High	PEAK	36	6000	2.24	1.00	134.4	1.89 (0.77)
	MpL	54	1340	10	1.00	134.4	0.98 (0.04)
	CL	41	140	100	1.04	134.4	1.11 (0.05)
	BpC	45	885.19	100	6.59	134.4	0.34 (0.22)

NA, not applicable.
[a] Velocity is outside of standard instrument clinical parameters (too fast).

researcher (S.A.L. or P.T.). Before dissection, non-pigmented choroidal specimens were excluded. During dissection, some tissues folded or tore from the mechanical arm and also were excluded. Thus, with four CBR specimens per globe, the total number of specimens tested was 620, and 516 samples met tissue quality criteria. Approximately 50 to 60 trials using each modality were performed.

Thermal Infrared Camera

High-resolution thermal imaging was performed using a FLIR camera (A655SC FLIR) with an attached lens (16 × 12 mm), creating a 25-μm zoom. Choroidal incisions were photographed immediately along with a calibrated ruler (engineering caliper; General Tools and Instruments LLC, Secaucus, NJ), by using a surgical microscope (Zeiss Universal S3 Opmi-6SFC; Carl Zeiss Meditec, Jena, Germany) and a digital camera (Exmor Full HD PMW-10MD; Sony Corp, Tokyo, Japan). Selective images were captured from video segments.

Calibration of the Thermal Camera

Thermal imaging from the thermal camera was calibrated and optimized by technical engineers before use. The emissivity of the tissue was calculated by comparing the emissivity of a reference compound (black electrical tape). As a result, the true emissivity of the tissue was derived by reference to standards calculated using FLIR software.

Image Analysis

ResearchIR Max software (55001-0302; FLIR) was used to interpret and analyze real-time thermal data outputs (Figs. 2A–D). Raw data were extracted from video recordings and included comma-separated value (CSV) files of temperature readings for every pixel per recorded frame. The number of frames analyzed per modality at each power setting is shown in Table 2. The testing period did not include the initial or final period of testing, which thus eliminated thermal heating variables. The CSV files also were created for average and maximum temperatures surrounding the probe/applicator tip of each modality. Python (Version 2.7.9), NumPy (Version 1.13), and Pandas (Version 0.18) were used to analyze the resulting CSV files. Thermal spread for each sample was calculated by analyzing each frame's CSV to determine the affected orthogonal distance from the path of tissue motion beneath each device (mm) using the threshold (cell death) temperature of $\geq 49°C$. The resulting mean (standard deviation [SD]) value from each frame was used with the rest of the sample's frames to calculate an overall mean (SD) thermal spread.

Statistical Analysis

Analysis of variance was used to determine significance between groups. Linear regression also was used to determine trends within groups. When possible, the data groups are presented as mean (SD). JMP 13 statistical software (SAS Institute, Inc., Cary, NC) was used for analysis, and $P < 0.05$ was
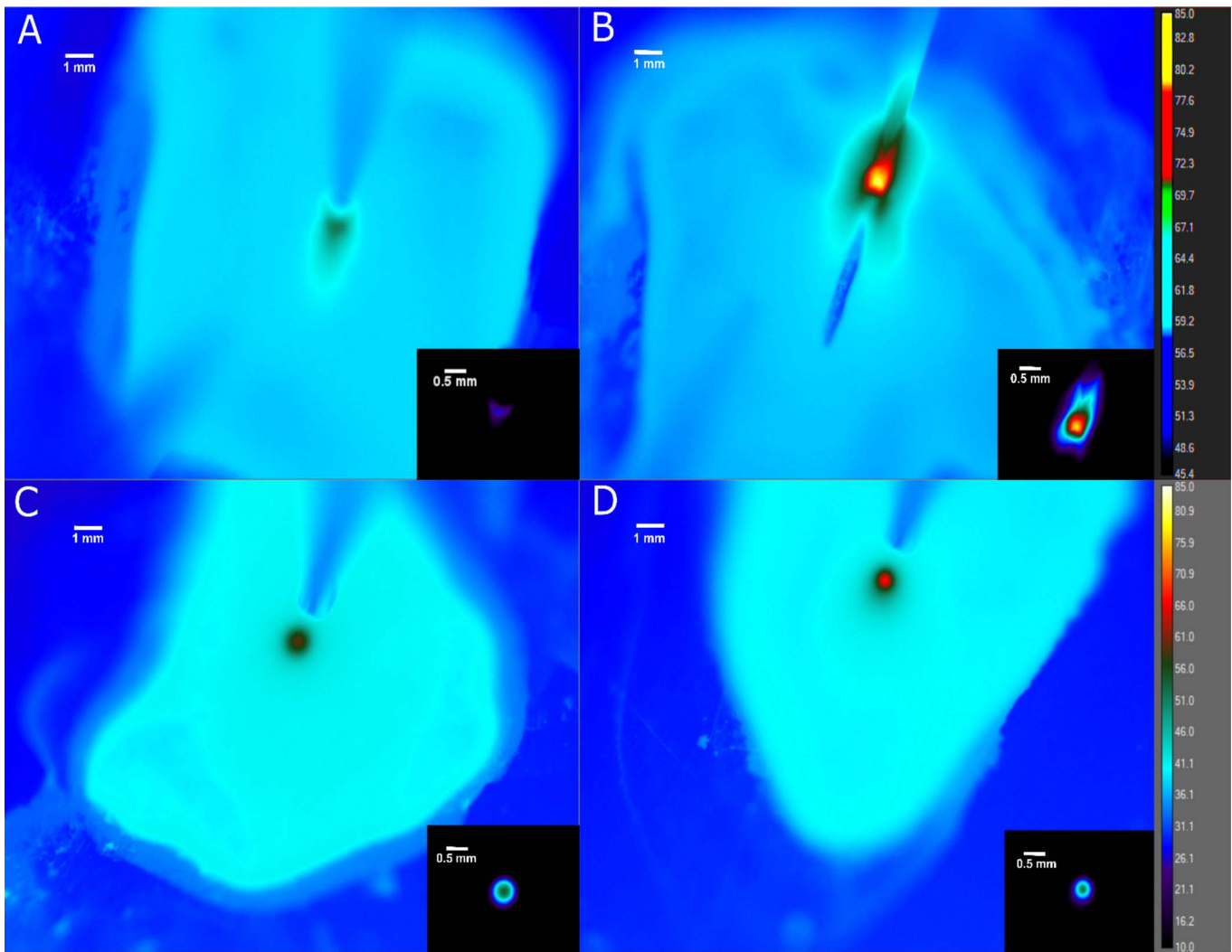
Figure 2. Temperature Change. (A–D) An A655SC infrared camera with an attached lens (16 × 12 mm) and a 25-μm zoom was used to measure temperature changes in CBR tissue. The devices tested were (A) BpC, (B) PEAK, (C) MpL, and (D) CL. All images represent the medium energy group (44.8 mJ/mm). Image insets represent changes in temperature ≥49°C (threshold for cell death). The *color grade scale* of the color pallet is in °C: the *top scale* refers to the *insets*, and the *lower scale* corresponds to the larger infrared images with a *blue background*.

considered statistically significant. A Tukey honestly significant difference test of the analysis of variance was performed post hoc to compare individual groups.

Results

Lateral Thermal Spread and Average Temperature

Between-group post hoc testing demonstrated significant differences in thermal spread between PEAK and MpL ($P < 0.001$), PEAK and BpC ($P < 0.001$), and PEAK and CL ($P < 0.001$) at all three energy levels (Fig. 3). Similarly, BpC was significantly different from

CL ($P < 0.001$) and MpL ($P < 0.001$) at medium and high energy levels. No significant differences in thermal spread were seen between MpL and CL on post hoc testing at low ($P = 0.38$), medium ($P = 0.86$), and high ($P = 0.36$) energy settings (Fig. 3). As predicted, an increase in power from all modalities resulted in increased lateral thermal spread and increased average temperature (both $P < 0.001$; Figs. 3, 4).

PEAK Analysis

To control for blade degradation over time, a new blade was used for each PEAK energy group, using a maximum of 35 short incisional passes per blade (based on the manufacturer's recommended device

Table 2. Thermal Camera Analysis

Energy Group	Device	Frames per Trial	Total Frames
Low[a]	PEAK	132.63 (37.73)	4642
	MpL	35.32 (6.30)	1766
	CL	34.48 (7.00)	1793
Medium	PEAK	171.50 (51.83)	10,290
	MpL	36.00 (1.59)	1800
	CL	49.98 (6.30)	2549
	BpC	66.71 (6.26)	3351
High	PEAK	166.68 (54.72)	4667
	MpL	21.48 (17.80)	1976
	CL	53.60 (35.22)	2519
	BpC	28.31 (7.05)	1472

[a] The BpC could not be adjusted to this energy level.

longevity). On post hoc analysis, the PEAK had the greatest thermal spread in all energy groups ($P <$ 0.001), with mean (SD) values of 0.23 (0.15), 0.97 (0.31), and 1.89 (0.77) mm in the low, medium, and high energy groups, respectively (Fig. 3).

In the low energy group, PEAK had decreasing temperature and thermal spread measurements with each successive application ($P < 0.001$; Figs. 5A, 6A). In the medium group, PEAK's lateral thermal spread was

significantly different between the two blades ($P < 0.05$; Fig. 5B). In the high energy group, PEAK demonstrated clinically relevant variation between disposable blades and thermal spread that was visibly, yet nonsignificantly, different between the blades ($P > 0.05$; Fig. 5C).

The lower energy PEAK did not reliably cut the CBR sample. In the medium and high energy groups, however, PEAK effectively incised CBR samples (Figs. 7A–C). Of note, bubbles were present above and below the tissue in both settings.

The shape and length of the electrode changed as a function of time in use and correlated with a decrease in tissue thermal output, thermal spread, and incision effectiveness (Fig. 8).

Spatial Variation of Thermal Analysis

To test the orientation of samples, we placed 55 samples perpendicular to and 46 parallel to the ora serrata. We studied MpL and CL on the high energy setting and saw no differences by tissue orientation using any measurable parameter with either method.

Discussion

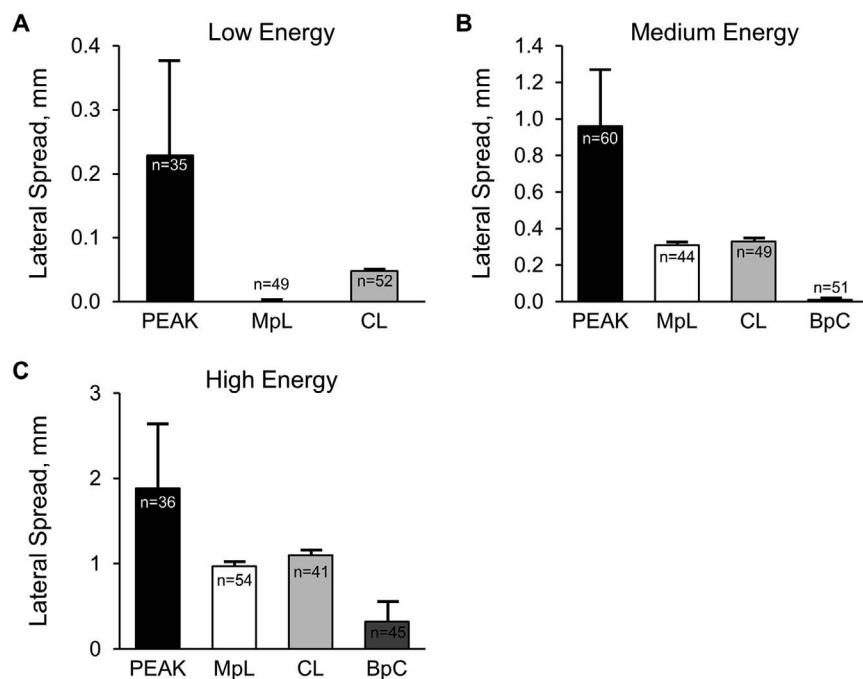Subretinal or suprachoroidal hemorrhage may develop during choroidal surgery and may lead to

Figure 3. Lateral thermal spread. Bar graphs show mean (SD) total lateral thermal spread in which tissue temperature was ≥49°C at three uniform power settings: (A) low (11 mJ/mm; note: the BpC bar is not shown), (B) medium (45 mJ/mm), and (C) high (134 mJ/mm) for all devices. $P < 0.001$ for all groups and comparisons except between CL and MpL at all energy groups ($P > 0.05$).
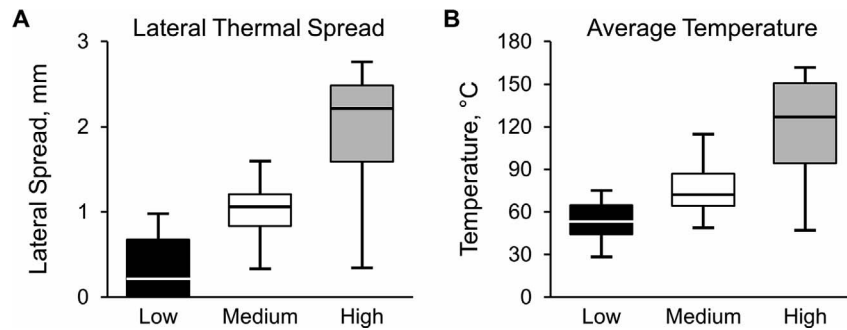
Figure 4. Box plots showing (A) lateral thermal spread and (B) average temperature for PEAK at low, medium, and high (11, 45, and 134 mJ/mm, respectively) energy groups. Both measures increased significantly with increasing energy ($P < 0.001$).

irreversible vision loss and other complications.[8–10] Devices that may achieve intraoperative hemostasis and avoid these complications are divided into several categories: laser modalities, electrosurgery (surgical diathermy), electrocautery (thermal cautery), and regulating the intraocular tamponade.[11,12] Also, endodiode laser thermal treatments along with endotamponade (during a chorioretinal biopsy)[13] and aggressive diathermy combined with systemic hypotension have been described previously.[14] All such methods (except tamponade), involve the application of thermal energy to limit intraocular bleeding, which may, in turn, lead to collateral tissue injury.

Our goal in designing a model to analyze this thermal tissue injury was to simulate the thermal energy transfer from ophthalmic devices into the highly vascular CBR tissue.[15,16] Although we did not fully recreate the intraocular, fluid-filled eye, our model allowed us to determine thermal tissue spread in a controlled environment and can be modified to simulate a fluid environment.

In our study, we analyzed and compared thermal spread from four modalities, each capable of addressing retinal and choroidal hemostasis: PEAK, MpL, CL, and BpC. Not surprisingly, we found that power output was directly proportional to the degree of lateral thermal spread, a finding supported by several studies.[17–19] However, the amount of tissue injury was
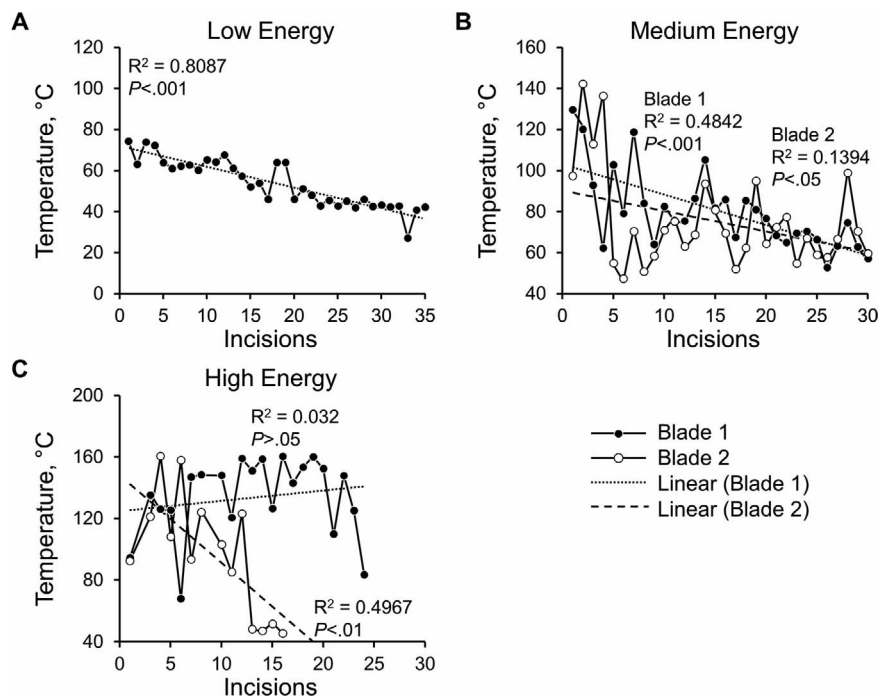

Figure 5. PEAK average temperature. Linear graphs of PEAK average temperature at low (A), medium (B), and high ([C]; 11, 45, and 134 mJ/mm, respectively) energy groups. A new blade was used after 30 incisions.
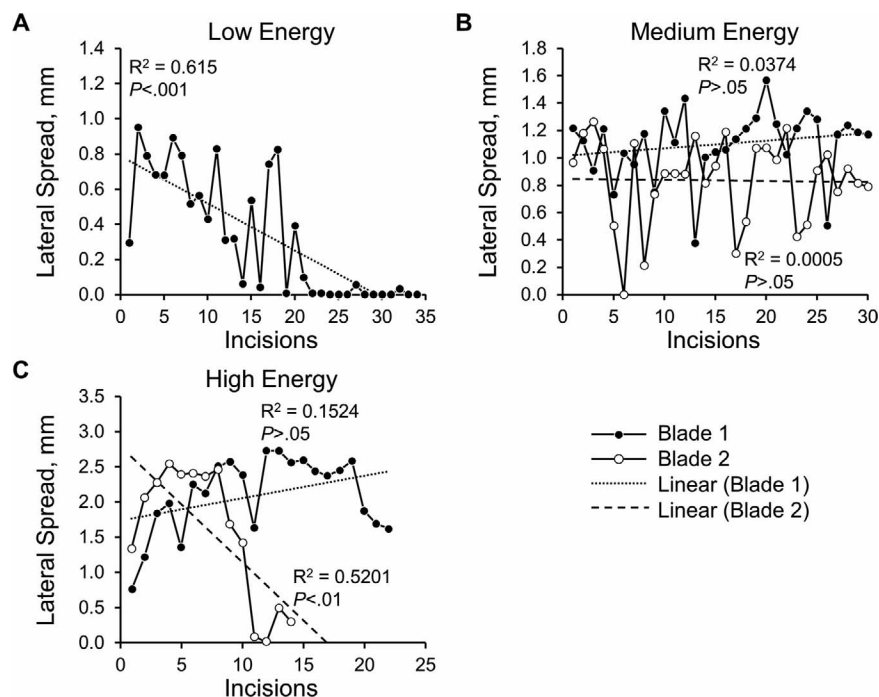
Figure 6. PEAK lateral thermal spread. Linear graphs of PEAK lateral thermal spread at low (A), medium (B), and high ([C]; 11, 45, and 134 mJ/mm, respectively) energy groups. A new blade was used after 30 incisions.

significantly different between devices using identical power output.

BpC and MpL had the least thermal spread at all three energy levels. We suspected the BpC would have a greater lateral thermal spread than the MpL because of its continuous power output and no duty cycle; however, this was not observed. Thermal energy delivery to the tissue may have been attenuated owing to the simulated study environment with BpC, in which the fluid-device interface is limited (moist, but not immersed in fluid), and less device-to-tissue heat transfer than may occur in a more standard fluid-enriched surgical environment (wet-field cautery). In most ophthalmologic surgical conditions, wet-field cautery is immersed in a saline, aqueous solution, especially in the posterior segment. Our rationale for minimizing the fluid interface was based on the measurement requirements of the infrared camera. Fluid irrigation would have added a cooling variable (i.e., the thermal effect measured is less than in clinical use) that was difficult to control. Also, there was a meaningful loss in thermal measurement sensitivity with increasing fluid medium.

The MpL had the next-lowest thermal impact across all three energy groups, and the measurements were repeatable. We anticipated that the MpL would have the lowest thermal propagation because of its precise area of energy application, combined with a low duty cycle. Subthreshold MpLs operate in short repetitive pulses of 100- to 300-microsecond intervals within an "envelope" lasting 0.1 to 0.5 seconds.[20] The envelope consists of a duty cycle; that is, the percentage of time when the laser is active within the envelope. Laser "on" time ranges from 5% to 15%.[20] During the laser "off" time, the tissue is able to cool, which limits thermal propagation into adjacent RPE, choriocapillaris, and surrounding tissue, especially when compared to CL applications at the same energy output.[21,22] We found significantly less thermal spread of the MpL compared to the CL in all energy groups (Table 1). We explained this by the equivalent total power output of the MpL and CL. In the clinical setting, a similar tissue effect could be obtained by using lower power settings on the MpL.

We used a subthreshold, 810-nm wavelength diode MpL. Other studies have shown that the 810-nm wavelength has a higher absorption in pigmented cells within the choroid.[23–26] Although hemostasis was not directly tested, the 810-nm diode MpL can potentially address the choroidal vasculature, even by directing the laser energy through transparent retina, while minimizing collateral thermal injury to the delicate RPE and neurosensory retina. Further testing of the MpL at lower power settings with in vivo studies will
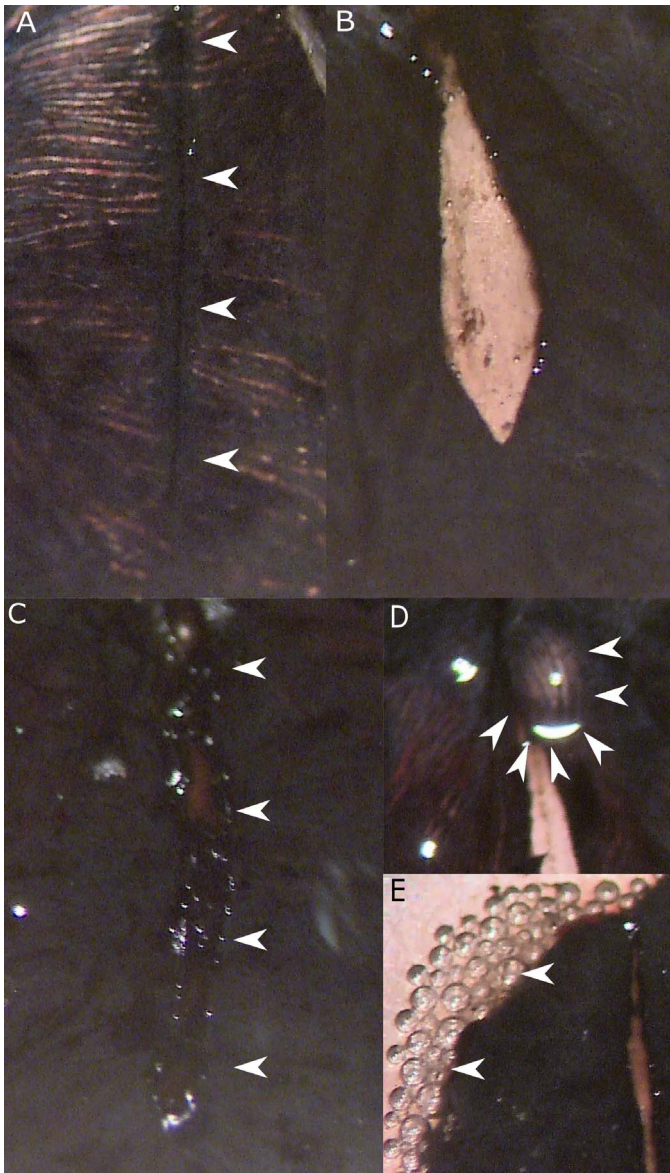
Figure 7. Incisions of the CBR with various powers of PEAK. (A) PEAK low-energy group disrupting the RPE (*arrowheads*). PEAK at medium (B) and high (C) energy demonstrating full-thickness choroidal incisions (*arrowheads*). Large (D) and small (E) cavitation bubbles (*arrowheads*) forming underneath the choroid.

Figure 8. PEAK tungsten electrodes. (A, B) Variation in the tip of the PEAK 12.5-μm tungsten electrode. (C) Tungsten electrode after 30 choroidal incisions, depicting a truncated blade tip (images do not correspond directly to the blades listed in Figure 5).

help confirm this theoretic advantage of MpL in the clinical-surgical setting.

The PEAK had the highest thermal spread of all modalities tested. Current PEAK devices have a much broader power range than we tested, and the energy output is adjusted for use in general surgery. The PEAK is the thinnest needle-delivery device. Although the power range is suboptimal for oph-thalmic purposes, output range varies greatly from 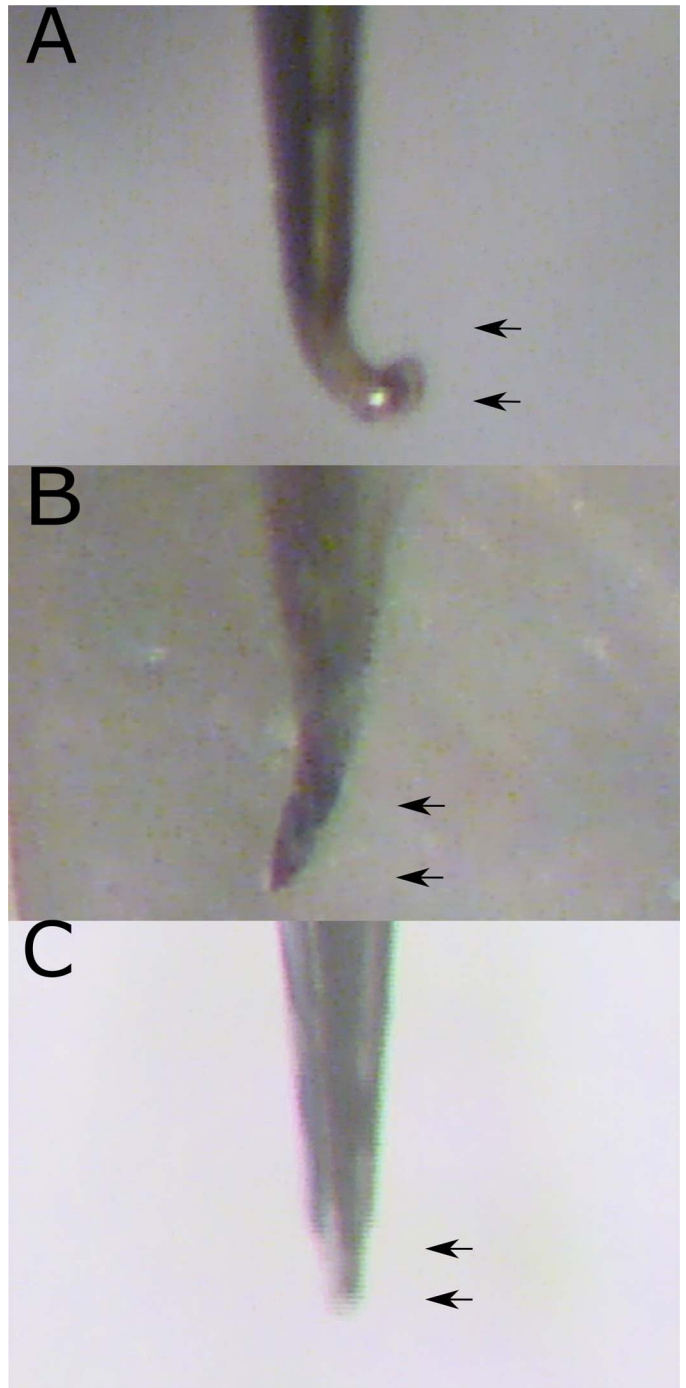the original PEAK for fine cutting (PEAK-fc), which produces incisions through the retina with up to 100 μm collateral tissue damage.[27,28] The histologic analysis underestimates thermal spread because damage is measured as a function of the highest temperature reached, along with the duration of

exposure.[29] Measuring the critical threshold temperature for permanent tissue damage is more likely to reflect the long-term effects on loss of delicate RPE and choriocapillaris. Our camera recorded the PEAK device to operate between the acceptable temperature ranges of 40°C and 170°C, as has been documented in other studies.[30]

The PEAK medium and high energy settings could effectively make full-thickness choroidal incisions, while also applying thermal energy for hemostasis; in comparison, at the low-energy setting, PEAK only disrupted the RPE cell layer (Figs. 7A–C). Visible collateral thermal damage was seen with PEAK at the high energy setting, but not the low or medium energies (Figs. 7A–C). Thus, we conclude that the PEAK medium output is the best energy level to provide the ideal cutting and coagulation required for incisional surgery through CBR tissue.

The PEAK is limited by the formation of cavitation bubbles, as were observed at the medium and high energy levels (Figs. 7D, 7E). PEAK technology causes the rapid evaporation of liquid, with explosive evaporation, resulting in shock waves and secondary cavitation bubbles.[31,32] Gas bubbles from the PEAK-fc are comparable in conventional electrosurgery.[27,28] In all PEAK blades we tested, we noted a change in the shape and length of the 12.5-μm tungsten electrode tip. Plasma microstreamers originate from the tungsten electrode and facilitate tissue dissection. Tungsten carbide is one of the most durable metals and is much harder than stainless steel.[33] Because the melting point of tungsten carbide is 3422°C, it is unlikely to melt at the operational temperature of this device (40°C–170°C). Interestingly, the shape of the tungsten electrode varied, even among new blades (Fig. 8).

We also analyzed the thermal spatial variation between laser modalities. Although we did not detect meaningful variation in temperature or thermal spread when changing tissue orientation, the size and color of posttreatment RPE distortion was not uniform. Others have noted that the ophthalmoscopic appearance of laser burns varies in size and color within the same eye, despite identical laser settings.[34,35] The variation seen in our data, similar to that of Yu et al.,[34] is most likely due to the normal variation of the choroidal and RPE pigmentation,[36] choroid thickness, or perhaps other unknown variables (e.g., choroidal blood flow that could not be tested in this model). Also, the two-dimensional thermographic profile limits our ability to determine the depth of thermal transfer.

We believe this information will be helpful clinically for techniques that require incision and hemostasis through the choroid. Minimizing collateral tissue loss of the delicate RPE and neurosensory retina is especially important when working near the macula or optic nerve, because such damage would certainly result in symptomatic loss of visual acuity or visual field, respectively. Others have shown that lasers create a visible burn that propagates from the original treatment zone, resulting in progressive RPE atrophy over time.[37] Thus, managing thermal energy spread during ocular procedures may lead to less surrounding tissue injury.

In our model to test ophthalmic surgical devices delivering thermal energy to fresh, ex vivo choroidal tissue and to measure the secondary injury using standardization of energy transfer, we tested four surgical devices. Each device was a candidate technology for effective choroidal hemostasis during incisional CBR surgery. We found that power output was directly proportional to the degree of lateral thermal spread. Also, tissue injury was significantly different between devices delivering identical power outputs. The MpL and BpC were the most effective for minimizing collateral thermal damage. However, we believed that our system underestimated the thermal spread of the BpC device, because a suboptimal fluid interface was required for the thermal camera to obtain reliable results. We understood that the decreased thermal spread was most likely due to an inadequate fluid interface. However, by adding irrigation to the tissue in the BpC group, we would add a variable that would alter the thermographics for this technology. The PEAK blade had the greatest thermal spread, yet also can create a full-thickness, tractionless incision through the choroid. Thus, BpC and PEAK offer substantial surgical advantages. The PEAK may be limited by cavitation bubble formation, especially at higher energy levels. MpL and CL had similar results, yet we believed that MpL may require lower power settings to achieve hemostasis in the clinical environment. Our data are clinically relevant for exploring approaches to incisional choroidal surgery with the goal of minimizing collateral tissue damage. We believed that our analysis has implications for surgical techniques, such as chorioretinal biopsies, tumor excisions, traumatic globe repair, macular translocation surgery, and potentially other macular-regenerative surgical approaches.

Acknowledgments

References

1. Alm A, Bill A. Ocular and optic nerve blood flow at normal and increased intraocular pressures in monkeys (Macaca irus): a study with radioactively labelled microspheres including flow determinations in brain and some other tissues. *Exp Eye Res*. 1973;15:15–29.

2. Auker CR, Parver LM, Doyle T, Carpenter DO. Choroidal blood flow. I. Ocular tissue temperature as a measure of flow. *Arch Ophthalmol*. 1982; 100:1323–1326.

3. Parver LM, Auker CR, Carpenter DO, Doyle T. Choroidal blood flow II. Reflexive control in the monkey. *Arch Ophthalmol*. 1982;100:1327–1330.

4. Alm A, Bill A. The oxygen supply to the retina. II. Effects of high intraocular pressure and of increased arterial carbon dioxide tension on uveal and retinal blood flow in cats. A study with radioactively labelled microspheres including flow determinations in brain and some other tissues. *Acta Physiol Scand*. 1972;84:306–319.

5. Charles ST. Controlled drainage of subretinal and choroidal fluid. *Retina*. 1985;5:233–234.

6. Denton ML, Noojin GD, Foltz MS, et al. Spatially correlated microthermography maps threshold temperature in laser-induced damage. *J Biomed Opt*. 2011;16:036003.

7. Iwami H, Pruessner J, Shiraki K, Brinkmann R, Miura Y. Protective effect of a laser-induced sublethal temperature rise on RPE cells from oxidative stress. *Exp Eye Res*. 2014;124:37–47.

8. Goldsmith C, Rene C. Massive spontaneous expulsive suprachoroidal haemorrhage in a blind glaucomatous eye treated with chronic topical steroid. *Eye (Lond)*. 2003;17:439–440.

9. Stein JD, Zacks DN, Grossman D, Grabe H, Johnson MW, Sloan FA. Adverse events after pars plana vitrectomy among Medicare beneficiaries. *Arch Ophthalmol*. 2009;127:1656–1663.

10. Garrott HM, Haynes RJ. Blindness from suprachoroidal haemorrhage in two patients with age-related macular degeneration on systemic anticoagulation therapy or an antiplatelet agent. *Med J Aust*. 2010;192:346–347.

11. Quiroz-Mercado H, Garza-Karren CD, Roigmelo EA, Jimenez-Sierra JM, Dalma-Weiszhausz J. Vitreous management in massive suprachoroidal hemorrhage. *Eur J Ophthalmol*. 1997;7:101–104.

12. Feretis E, Mourtzoukos S, Mangouritsas G, Kabanarou SA, Inoba K, Xirou T. Secondary management and outcome of massive suprachoroidal hemorrhage. *Eur J Ophthalmol*. 2006;16: 835–840.

13. Cole CJ, Kwan AS, Laidlaw DA, Aylward GW. A new technique of combined retinal and choroidal biopsy. *Br J Ophthalmol*. 2008;92: 1357–1360.

14. Peyman GA, Juarez CP, Raichand M. Full-thickness eye-wall biopsy: long-term results in 9 patients. *Br J Ophthalmol*. 1981;65:723–726.

15. Weiter JJ, Ernest JT. Anatomy of the choroidal vasculature. *Am J Ophthalmol*. 1974;78:583–590.

16. Parver LM, Auker C, Carpenter DO. Choroidal blood flow as a heat dissipating mechanism in the macula. *Am J Ophthalmol*. 1980;89:641–646.

17. Sutton PA, Awad S, Perkins AC, Lobo DN. Comparison of lateral thermal spread using monopolar and bipolar diathermy, the Harmonic Scalpel and the Ligasure. *Br J Surg*. 2010;97:428–433.

18. Hefermehl LJ, Largo RA, Hermanns T, Poyet C, Sulser T, Eberli D. Lateral temperature spread of monopolar, bipolar and ultrasonic instruments for robot-assisted laparoscopic surgery. *BJU Int*. 2014;114:245–252.

19. Druzijanic N, Pogorelic Z, Perko Z, Mrklic I, Tomic S. Comparison of lateral thermal damage of the human peritoneum using monopolar diathermy, Harmonic scalpel and LigaSure. *Can J Surg*. 2012;55:317–321.

20. Dorin G. Subthreshold and micropulse diode laser photocoagulation. *Semin Ophthalmol*. 2003; 18:147–153.

21. Sivaprasad S, Elagouz M, McHugh D, Shona O, Dorin G. Micropulsed diode laser therapy: evolution and clinical applications. *Surv Ophthalmol*. 2010;55:516–530.

22. Angioletti LV, Yellen MJ. Preliminary results of ICG dye-enhanced micro-pulsed laser photocoagulation of subfoveal choroidal neovascular

membranes in age-related macular degeneration. *Lasers Surg Med.* 1995;17:29.

23. McHugh JDA, Marshall J, Ffytche TJ, Hamilton AM, Raven A. Macular photoagulation of human retina with a diode laser: a comparative histopathological study. *Lasers Light Ophthalmol.* 1990;3:11–28.

24. Vogel A, Birngruber R. Temperature profiles in human retina and choroid during laser coagulation with different wavelengths ranging from 514 to 810 nm. *Lasers Light Ophthalmol.* 1992;5:9–16.

25. Peyman GA, Raichand M, Zeimer RC. Ocular effects of various laser wavelengths. *Surv Ophthalmol.* 1984;28:391–404.

26. Friberg TR, Karatza EC. The treatment of macular disease using a micropulsed and continuous wave 810-nm diode laser. *Ophthalmology.* 1997;104:2030–2038.

27. Priglinger SG, Haritoglou C, Mueller A, et al. Pulsed electron avalanche knife in vitreoretinal surgery. *Retina.* 2005;25:889–896.

28. Priglinger SG, Haritoglou C, Palanker DV, Alge CS, Gandorfer A, Kampik A. Pulsed electron avalanche knife (PEAK-fc) for dissection of retinal tissue. *Arch Ophthalmol.* 2005;123:1412–1418.

29. Campbell PA, Cresswell AB, Frank TG, Cuschieri A. Real-time thermography during energized vessel sealing and dissection. *Surg Endosc.* 2003;17:1640–1645.

30. Palanker DV, Vankov A, Huie P. Electrosurgery with cellular precision. *IEEE Trans Biomed Eng.* 2008;55:838–841.

31. Peng Q, Juzeniene A, Chen J, et al. Lasers in medicine. *Rep Prog Phys.* 2008;71:056701.

32. Vogel A, Busch S, Jungnickel K, Birngruber R. Mechanisms of intraocular photodisruption with picosecond and nanosecond laser pulses. *Lasers Surg Med.* 1994;15:32–43.

33. Mechanical properties of the elements. In: Samsonov GV, ed. *Handbook of the Physicochemical Properties of the Elements.* New York, NY: IFI/Plenum; 1968:387–445.

34. Yu AK, Merrill KD, Truong SN, Forward KM, Morse LS, Telander DG. The comparative histologic effects of subthreshold 532- and 810-nm diode micropulse laser on the retina. *Invest Ophthalmol Vis Sci.* 2013;54:2216–2224.

35. Wood EH, Karth PA, Sanislo SR, Moshfeghi DM, Palanker DV. Nondamaging retinal laser therapy for treatment of central serous chorioretinopathy: what is the evidence? *Retina.* 2017;37:1021–1033.

36. Pollack JS, Kim JE, Pulido JS, Burke JM. Tissue effects of subclinical diode laser treatment of the retina. *Arch Ophthalmol.* 1998;116:1633–1639.

37. Dorin G. Evolution of retinal laser therapy: minimum intensity photocoagulation (MIP). Can the laser heal the retina without harming it? *Semin Ophthalmol.* 2004;19:62–68.